POLITECNICO DI TORINO
Repository ISTITUZIONALE

Development and Characterization of New Functionally Graded Aluminium Alloys

Original
Development and Characterization of New Functionally Graded Aluminium Alloys / Fracchia, E., Rosso, M. - In: Aluminium Alloys - Design and Development of Innovative Alloys, Manufacturing Processes and Applications / Timelli G.. - ELETTRONICO. - [s.l] : IntechOpen, 2022. - ISBN 978-1-83968-729-7. - pp. 1-19 [10.5772/intechopen.101022]

Availability:
This version is available at: 11583/2936594 since: 2022-07-22T13:55:01Z

Publisher:
IntechOpen

Published
DOI:10.5772/intechopen.101022

Terms of use:

This article is made available under terms and conditions as specified in the corresponding bibliographic description in the repository

Publisher copyright

(Article begins on next page)

20 November 2026

We are IntechOpen, the world's leading publisher of Open Access books Built by scientists, for scientists

5,500
Open access books available

135,000
International authors and editors

165M
Downloads

Our authors are among the

154
Countries delivered to

TOP 1%
most cited scientists

12.2%
Contributors from top 500 universities

CLARIVATE ANALYTICS
BOOK CITATION INDEX
INDEXED

WEB OF SCIENCE™

Selection of our books indexed in the Book Citation Index in Web of Science™ Core Collection (BKCI)

Interested in publishing with us?
Contact book.department@intechopen.com

Numbers displayed above are based on latest data collected.
For more information visit www.intechopen.com

Chapter

Development and Characterization of New Functionally Graded Aluminium Alloys

Elisa Fracchia and Mario Rosso

Abstract

Nowadays, aluminium alloys are adopted mainly to produce engineering and automotive components. The present investigation aims to design, cast and characterize novel functionally graded materials (FGMs) produced using Al-Mg and Al-Si alloys by gravity casting technique. Alloys were sequentially cast into a mould to obtain an FGM to realizing great mechanical and metallurgical bonding. Zn addition was further performed in FGM to increase the mechanical properties, thanks to the nucleation of the intermetallic phases $MgZn_2$. Castings were subsequently mechanically tested by tensile tests, bending tests, hardness and microhardness measures to assess the products' quality. Microstructural characterizations were performed along the FGM to assess the metallurgical bonding and evaluate the microstructures obtained. Fracture, microstructural and compositional analysis will highlight the quality of this new FGM proposed. Possible applications of these materials are suggested, as automotive pistons or structural components.

Keywords: FGM, Al-Si alloy, Al-Mg alloy, tensile tests, bending test, microstructures, SEM analysis

1. Introduction

The last few decades were characterized by significant growth of the aluminium market. This growing interest in aluminium alloys is attributable to their excellent properties such as good or excellent specific mechanical strength, lightweight and generally good corrosion resistance [1]. During previous years, in the automotive market, these properties have allowed replacing some heavy components made in steel with the same components made in aluminium, leading to cost savings, structural lightening and CO_2 emission reduction. However, if, on the one hand, aluminium alloys have good properties that permit the production of components with homogenous characteristics providing high performances, on the other hand, some applications may require specific features as graded structures. Functionally graded materials (FGMs) have graded structures characterized by different compositions or microstructures, as deeply investigated in [2]. In particular, gradient types were classified as chemical composition gradients, porosity gradients or microstructural gradients [3], while microstructural gradients are further subdivided

into fraction gradient, shape gradient, orientation gradient and size gradient [4]. Various production methods such as powder metallurgy, centrifugal casting, vapour deposition [5] or additive manufacturing [6] can be used to produce FGMs. FGMs usage involves various markets, such as biomedical, chemical, aerospace, electronics, nuclear or energy; for instance, in [7], the powder metallurgy method was used, and the authors successfully fabricated a porosity gradient Ti-Zr FGM for biomedical application.

As aluminium-FGMs regard, various publications concern the functionally graded metal-ceramic composites rather than metal-metal ones. In [8], authors realized a layered Al-SiC FGM by powder metallurgy technique. Each layer was composed of different SiC content, and the consolidation between each layer was assured by cold compaction. Similarly, in [9] a layered Al-Al_2O_3 FGM was suggested. Other manuscripts suggest the adoption of Al alloys instead of the commercially pure aluminium powder. In particular, in [10], FGM produced with aluminium alloy A7075 was suggested for gears or brake drums. In addition to powder metallurgy, FGMs may be prepared in other ways: in [11], authors proposed the centrifugal casting technique to realize A356-SiC FGMs. The mould rotation permits a radial distribution of SiC particles, and in the end, the samples could be distinguished into three different zones—reinforced zone (outer zone), transitional zone (middle zone) and the unreinforced alloy (inner zone). Centrifugal casting was also successfully adopted in [12] to produce automotive pistons by adopting two aluminium alloys—A336 and A242. As centrifugal casting regards, different production parameters must be considered, as pointed up in the review article [13].

On the other hand, gravity casting is a newish casting method used to produce FGMs. In [14], the authors used gravity casting to realize two metal-metal FGM, adopting the aluminium alloys A390-A319 (both casting alloys) and A390-A6061 (casting and wrought alloys). In particular, to obtain a good metallurgical bonding between alloys, some casting parameters were carefully monitored, as the time gap during sequential pouring and the pouring temperature. In this work, metal-metal FGMs were realized by controlling the mould filling using gravity casting [15]. Alloys EN AC 47000 and EN AC 51100 were used, with and without Zn addition, to assess the mechanical properties and the metallurgical bonding in this new kind of FGM. FGMs properties were then compared to the properties of the single alloys.

2. Materials and methods

2.1 Materials

Aluminium alloys adopted to realize FGMs are EN AC 47000 and EN AC 51100. Details about alloys chemical composition are reported in **Table 1**. Alloy EN AC 51100 (AlMg3) has a wide range of applications in the automotive industry; Mg increases corrosion resistance and solution hardening [16].

EN AC 47000 (AlSi12(Cu)) is a eutectic alloy having Si as the primary alloying element. Si and Cu increase mechanical properties, in particular after heat treatment.

Commercially pure Zn ingot was used as an alloying element in a quantity of 1.5 w.t.% in some specific samples.

2.2 FGM production

FGMs were realized by controlling the mould filling during the gravity casting [17, 18]. The alloys are melted in two different crucibles while the mould is painted

EN AC 47000							
w.t.%	Cu	Mg	Si	Fe	Mn	Zn	Al
	0.62	0.09	12.98	0.54	0.26	0.47	Bal.
EN AC 51100							
w.t.%	Cu	Mg	Si	Fe	Mn	Zn	Al
	0.042	2.786	0.432	0.285	0.188	0.049	Bal.

Table 1.
FGM alloys composition.

with BN-based stop off-paint and preheated at 400°C. The mould is a C40 steel mould having dimensions 85 mm (depth) × 200 mm (height) × 15 mm (width). The alloys were poured in a precise amount to fill half of the mould figures (see dotted lines in **Figure 1A** and **B**). Approximately 150 g of EN AC 51100 alloy was poured at 710°C into the mould, as indicated by the orange arrow in **Figure 1A**, filling half of it. After the first casting, 185 g of alloy EN AC 47000 was poured, at 710°C, over EN AC 51100 to fill the second half of the mould, as shown in **Figure 1B**. The pouring of alloy EN AC 47000 was performed without any time delay after casting the first composition. Castings are manually extracted from the mould in the fastest way possible by using pullers and then quenched in water at 25°C; the manual extraction method may cause little change in cooling rate (that was not specifically measured) between subsequent castings. Because of the mould shape, there is no specific pouring channel for the second alloy, EN AC 47000, which must be poured into two different parts of the mould, as indicated in **Figure 1B**. This mould configuration may affect the junction tightness inside castings, causing the presence of gas porosities

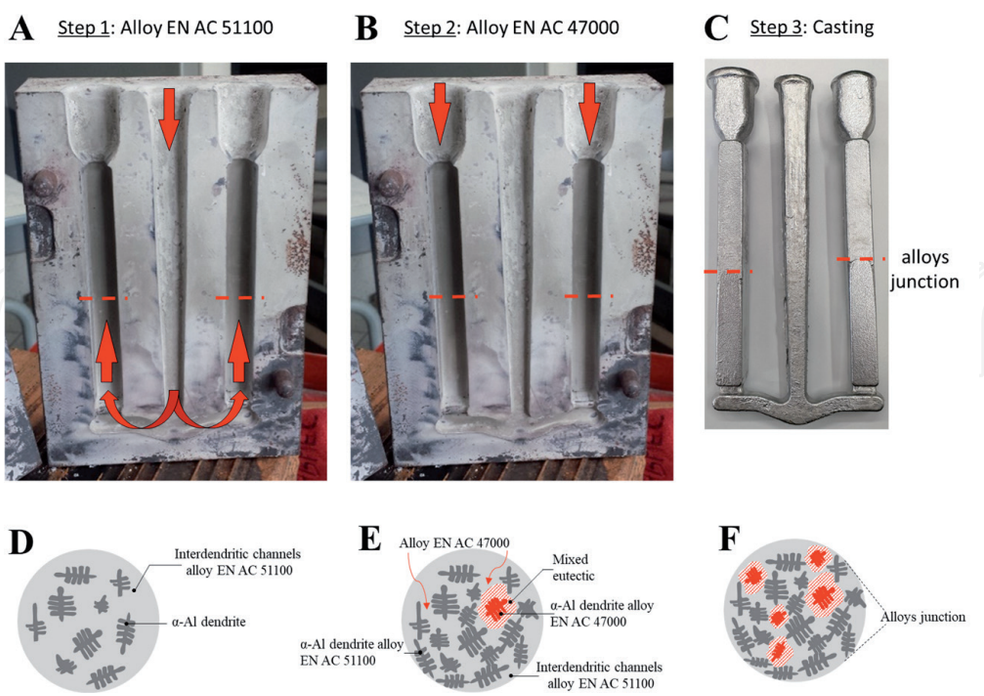


Figure 1.
Filling operations. A: Step 1, half-mould image; the casting of alloy EN AC 51000 inside the mould carried out as indicated by the orange arrow. B: Step 2, casting alloy EN AC 47000 inside the mould carried out as indicated by orange arrows. C: Step 3, casting obtained. D: Step 1 of casting, nucleation of α-Al dendrites near nucleation site and mould walls after the casting of composition EN AC 51100. E: Step 2 of casting, nucleation of α-Al dendrites of alloy EN AC 47000 into the interdendritic channels of alloy EN AC 51100 previous poured. F: EN AC 47000 alloy into the interdendritic channels of alloy EN AC 51100 after the pouring.

Castings	Alloys	Casting details
#1	FGM. EN AC 51100 and EN AC 47000	—
#2	FGM. EN AC 51100 and EN AC 47000 + 1.5w.t.% Zn	1.5w.t.% Zn in alloy EN AC 47000 (~ 2.8 g)
#3	FGM. EN AC 51100 + 1.5w.t.% Zn and EN AC 47000 + 1.5w.t.% Zn	Zn in EN AC 47000 (~ 2.8 g) and in EN AC 51100 (~ 2.2 g)
#4	Single alloy EN AC 47000 + 1.5w.t.% Zn	Zn addition (~ 2.8 g)
#5	Single alloy EN AC 51100 + 1.5w.t.% Zn	Zn addition (~ 2.2 g)
#6	Single alloy EN AC 51100	—
#7	Single alloy EN AC 47000	—

Table 2.
Experimental conditions.

and oxides. An example of the casting obtained is shown in **Figure 1C**. Each FGM bar measures 25 mm (depth) × 125 mm (height) × 15 mm (width), and the interface between alloys is approximately placed in the middle.

As mechanical properties are relevant in automotive FGM, Zn addition was performed to increase mechanical strength. For this reason, three different types of FGM were realized—FGM without Zn, FGM with Zn addition in alloy EN AC 47000 and finally FGM with Zn addition in both the alloys. Moreover, in order to evaluate the alloys' mechanical properties, single-alloy specimens have been cast, with and without Zn addition. The different experimental conditions are summarized in **Table 2**.

2.3 Mechanical and microstructural tests

With the aim to evaluate the mechanical properties of the produced FGMs and compare them with those of the single alloys, tensile tests, three-point bending tests and microhardness measures were made. Tensile tests were performed following the norm ASTM B557–15. Specimens were machined in a plate dog-bone shape from the rectangular castings; in FGM tensile specimens, the interface between the alloys was placed in the middle of the samples. Since the properties of the FGM without Zn addition are the work's focus, a higher number of the tensile test specimens were produced. Overall, these were realized six specimens for this type of FGMs without Zn, while the other types of casting were machined with two samples.

Three-point bending tests were performed on bar measures 10 mm × 10 mm × 60 mm, adopting a support span of 40 mm, test speed 0.004 1/s and a preload of 5 N. During the tests, the load is applied in the middle of the specimens, while on the opposite side the sample is supported by two wedges. In FGM bending specimens, the interface between the alloys was placed in the middle of the samples. Overall, there were six specimens for FGMs without Zn, while the other FGMs were machined in two samples. Four specimens were tested for the single alloys (castings with and without Zn).

Microhardness Vickers tests were performed on each specimen. FGMs interfaces were subjected to a microhardness matrix 8 × 8; the distance between each indentation was 150 μm, the applied load was 15 gf for 15 s and the diagonal was measured after the indentation varies almost from 25 to 35 μm. Single alloys were also tested, performing five indentations for each sample. Microhardness was chosen instead of Vicker hardness because it may be more sensitive to the slight hardness variations near the interface of the FGM samples. In fact, the junction areas of alloys are pretty low, of a few hundred microns.

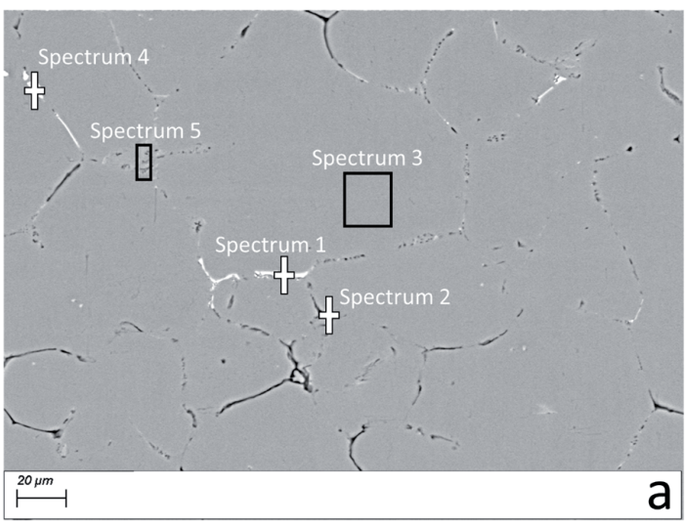
Microstructures were evaluated through SEM microscope, and EDS semiquantitative analyses were also carried out. Castings were cut and polished by using SiC papers

from 180 to 2500 grit, and then, colloidal silica having a granulometry of 0.03 μm was used for mirror-polishing. Finally, specimens were etched with Keller's reagent. Fracture surfaces after tensile tests were also investigated through SEM analysis.

3. Results and discussion

3.1 Intermetallic phases

Figure 2 shows microstructures obtained at SEM microscope for specimens of alloy EN AC 51100 with Zn and EN AC 51100 without Zn addition. Different intermetallic phases are noticeable from **Figure 2a**: Al-Fe-Mn-Si phases (spectrums 1 and 4), the eutectic α-Al/Al_3Mg_2 phase (spectrum 5) and Mg_2Si phase (spectrums 2 and 5). Mainly, Al_3Mg_2 is characterized by the typical acicular shape and the black colour, as in spectrum 2 [16]. Mg_2Si can be present inside the eutectic α-Al/Al_3Mg_2 phase (grey precipitations). Similar results were noticed in **Figure 2b** for the analysed specimen of alloy EN AC 51100 with Zn addition. In particular, Zn was detected in spectrums 3, 4 and 5, along with Mg and Si. White intermetallic



Spectrum 1

Elements	Wt%
Al	70.6
Fe	11.9
Si	8.9
Mn	7.8
Cu	0.4
Mg	0.4

Spectrum 4

Elements	Wt%
Al	73
Fe	10.9
Si	8.1
Mn	8.0

Spectrum 2

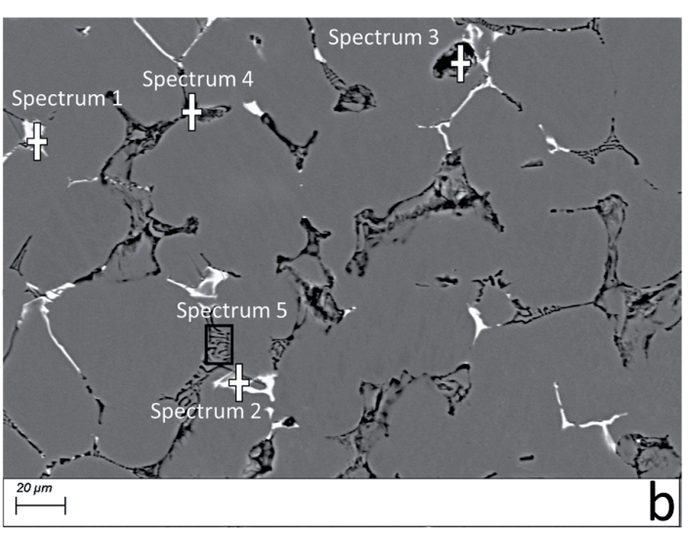
Elements	Wt%
Al	78.7
Si	20.8
Mg	0.5

Spectrum 5

Elements	Wt%
Al	77.0
Si	20.3
Mg	2.7

Spectrum 3

Elements	Wt%
Al	98.1
Mg	1.2



Spectrum 1

Elements	Wt%
Al	70.6
Fe	19.1
Si	6.1
Mn	3.8
Mg	0.5

Spectrum 4

Elements	Wt%
Al	90.9
Si	4.0
Mg	3.8
Zn	1.2

Spectrum 2

Elements	Wt%
Al	66.3
Fe	22.2
Si	6.7
Mn	4.9

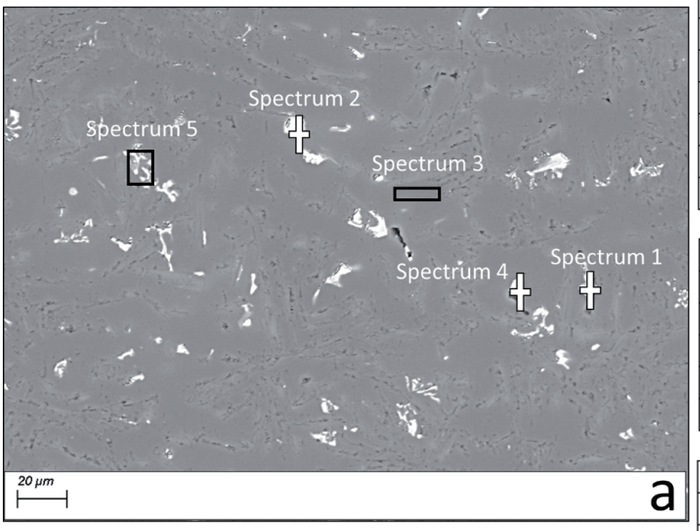
Spectrum 5

Elements	Wt%
Al	90.5
Si	4.8
Mg	4.0
Zn	0.8

Spectrum 3

Elements	Wt%
Al	95.8
Mg	2.8
Zn	0.9
Si	0.4

Figure 2.
SEM-EDS analysis of specimen EN AC 51100 (a) and EN AC 51100 + Zn (b).



Spectrum 1

Elements	Wt%
Al	60.0
Cu	15.3
Fe	11.0
Si	9.3
Mn	2.7
Mg	1.8

Spectrum 4

Elements	Wt%
Al	54.2
Cu	28.2
Si	10.6
Mg	7.0

Spectrum 2

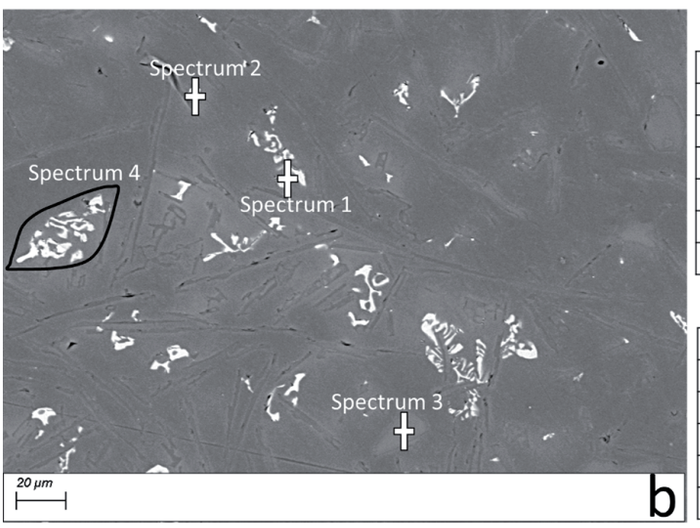
Elements	Wt%
Al	59.9
Fe	19.5
Si	9.9
Mn	9.4
Cu	1.2

Spectrum 5

Elements	Wt%
Al	77.3
Fe	8.0
Si	7.8
Mn	3.5
Mg	1.8
Cu	1.6

Spectrum 3

Elements	Wt%
Al	66.4
Si	33.6



Spectrum 1

Elements	Wt%
Al	62.9
Fe	17.5
Si	9.2
Mn	8.2
Zn	1.2
Cu	1.0

Spectrum 3

Elements	Wt%
Si	99.2
Al	0.8

Spectrum 2

Elements	Wt%
Al	58.3
Cu	32.0
Si	4.5
Mg	3.1
Zn	2.0

Spectrum 4

Elements	Wt%
Al	82.6
Si	7.5
Fe	2.9
Cu	2.8
Zn	2.8
Mn	1.5

Figure 3.
SEM-EDS analysis of specimen EN AC 47000 (a) and EN AC 47000 + Zn (b).

compounds contain a high amount of Fe and Mn were also noticed in **Figure 2a** spectrum 4 and **Figure 2b** spectrum 2, identifiable as α-Al (Fe, Mn) Si phase.

Figure 3 shows microstructures obtained at SEM microscope for specimens of alloy EN AC 47000 with Zn and EN AC 47000 without Zn addition. In **Figure 3a**, white intermetallic compounds contain Fe, Mn and Cu, (spectrums 1, 2 and 5) similar to those observed in alloy EN AC 51100 were observed. Spectrum 4 is an intermetallic phase Al-Si-Mg-Cu also known as Q phase [19]. Similarly, intermetallic phases detected in **Figure 3b** highlight the presence of the Q phase in spectrum 2. Spectrum 3 highlights a eutectic silicon polygonal particle. The Zn was noticed in the intermetallic Fe-based, commonly known as Chinese script, α-AlFeSiCuMg.

3.2 FGMs interfaces

Figure 4 reports the SEM-EDS maps of the FGMs interfaces obtained. **Figure 4a** highlights the Si diffusion into Mg-based alloy, especially into the eutectic regions α-Al/Al_3Mg_2.

Iron-based intermetallic compounds are largely diffused into EN AC 47000 alloy, as noticeable from the maps; furthermore, Mg was detected in both the alloys with a slight depletion at the interface. Although Si was detected at the interface

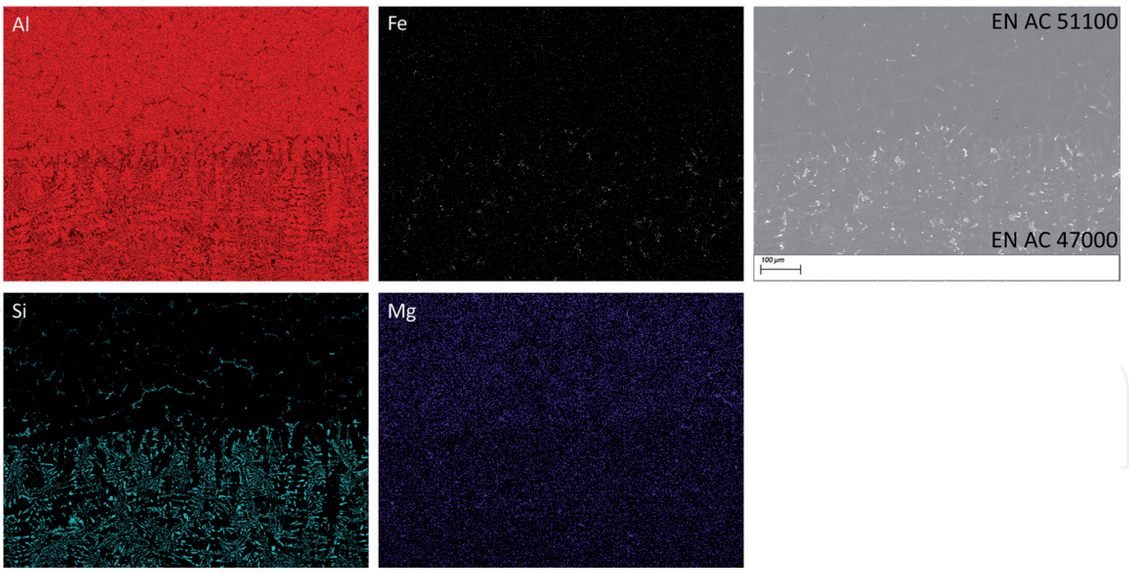


Figure 4.
EDS maps analysis in FGM without Zn interface.

into the EN AC 51100 bulk, in the alloy bulk Si was noticed only in a few intermetallic phases. In fact, EDS map analysis conducted into the EN AC 51100 bulk did not evidence appreciable amounts of silicon, as is possible to note in **Figure 5**.

After Zn addition, Zn-based intermetallic compounds are detected. **Figure 6** shows the SEM-EDS maps for FGM with Zn addition in alloy EN AC 47000. Overall, it seems that the Zn amount was not enough to be appreciated in the EDS maps near the interface; on the other hand, Zn was clearly noticed in the bulk alloy of the sample made in single alloy EN AC 47000 + Zn, as is shown in **Figure 7**.

Interface maps for FGM containing Zn in both alloys clearly show the presence of Zn, with a slight depletion into the interface between the compositions (see **Figure 8**). Furthermore, as also noticed in the other FGMs, Mg depletion was observed near the alloy interface. This depletion may be explained considering the alloy mixing that took place during the pouring of the second composition; in fact, near the interface, these were mainly noticed iron-based intermetallic phases (**Figures 4** and **6**).

No defects such as oxide layers or shrinkage were observed in the FGM interfaces.

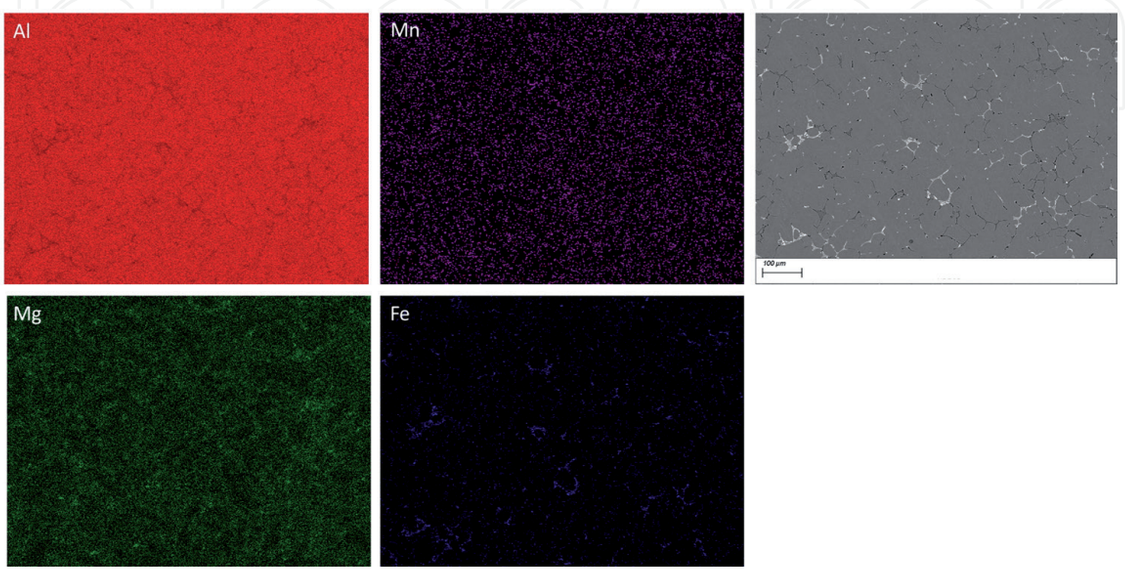


Figure 5.
EDS maps analysis of EN AC 51100 bulk.

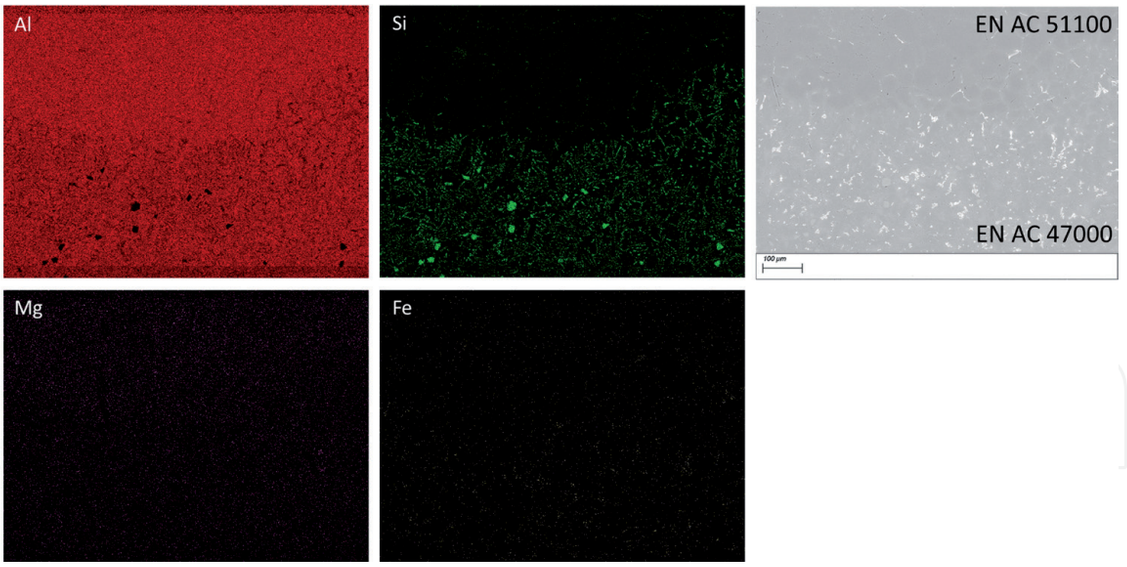


Figure 6.
EDS maps analysis in FGM (with Zn addition in alloy EN AC 47000) interface.

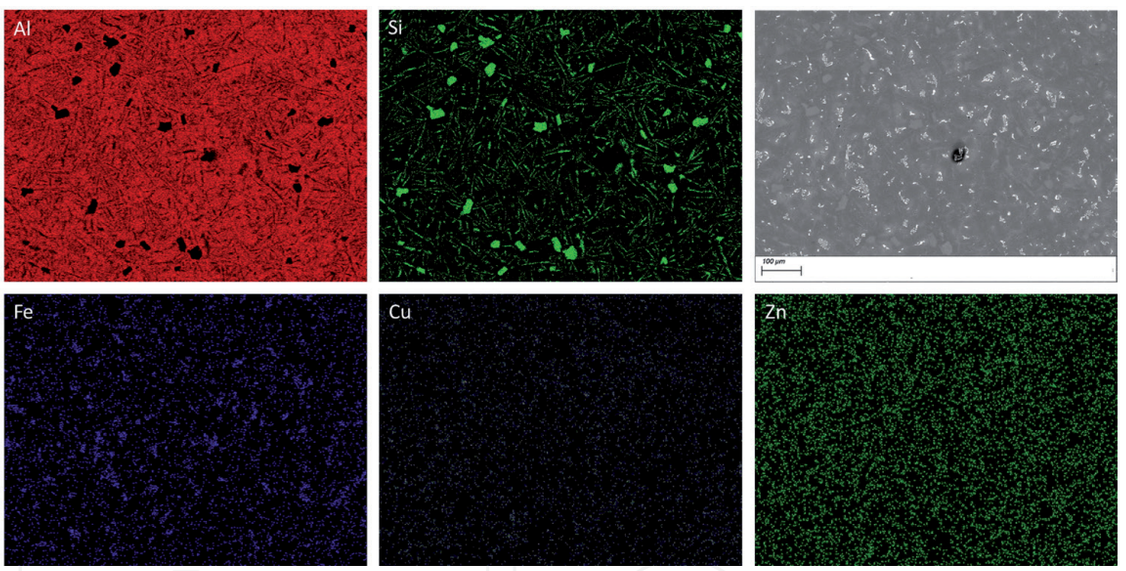


Figure 7.
EDS maps analysis of EN AC 47000 bulk.

3.3 Mechanical tests

3.3.1 Microhardness

Microhardness measured in alloys with and without Zn additions is shown in the bar chart of **Figure 9**. As FGMs regard, the microhardness matrixes measured through the interfaces are shown in **Figure 10**.

Average interface hardness appears similar in FGM and in FGM with Zn addition in alloy EN AC 47000, respectively 72 ± 16 HV0.15 and 69 ± 15. On the other hand, in the FGM with Zn addition in both alloys, the interface was characterized by a higher average microhardness, of almost 81 ± 16.

Overall, the standard deviations in FGM specimens are similar (16, 15 and 16). The same behaviours were observed in alloy EN AC 47000, with and without Zn additions. Microhardness measured in EN AC 47000 was 95 ± 12 HV0.15 without Zn addition and 80 ± 12 HV0.15 with Zn addition.

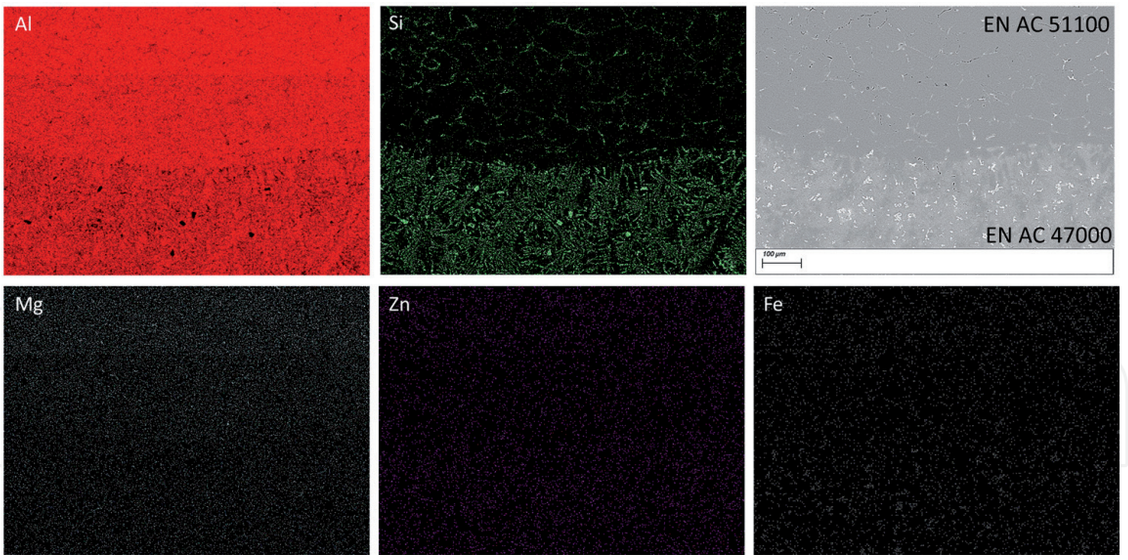


Figure 8.
EDS maps analysis in FGM (with Zn addition in both the alloys) interface.

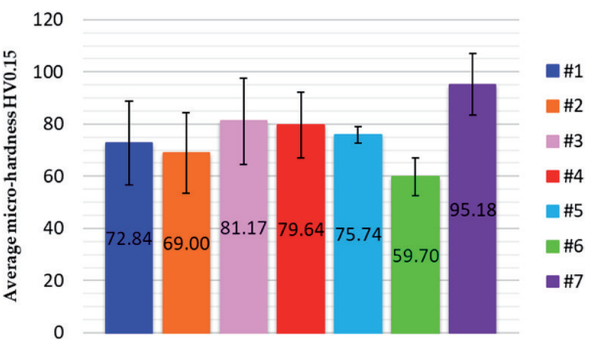


Figure 9.
Average microhardness measured in bulk alloys EN AC 47000 + Zn, EN AC 51100 + Zn, EN AC 47000, EN AC 51100 (bars 4, 5, 6, 7) and average microhardness measured for FGM, FGM with Zn addition in EN AC 47000 and FGM with Zn addition in both alloys (bars 1, 2, 3).

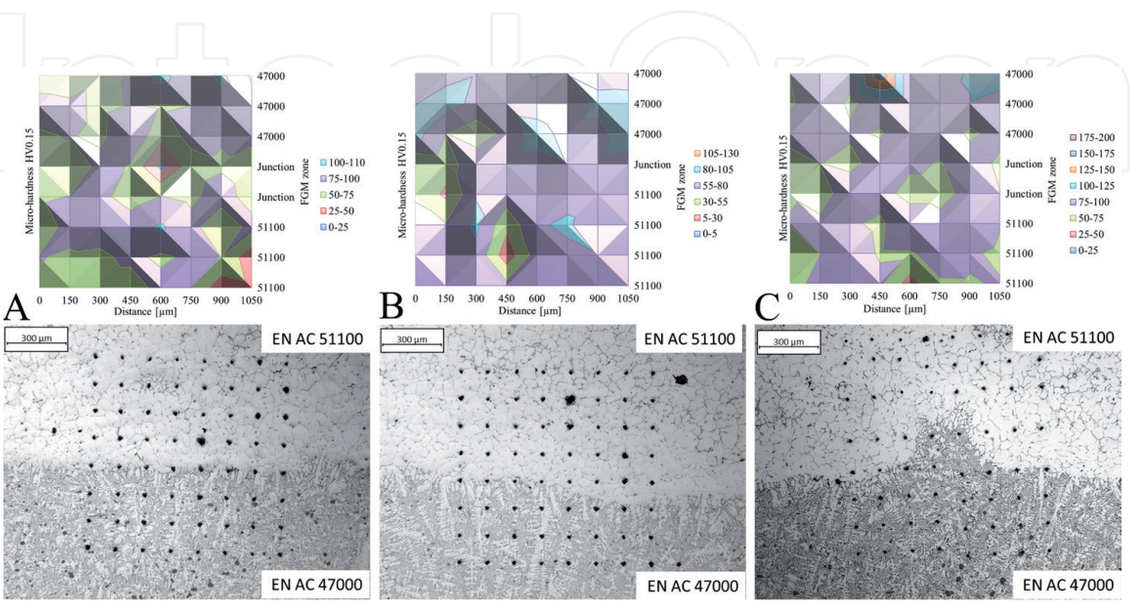


Figure 10.
Microhardness maps for FGMS. A: FGM; B: FGM with Zn addition in EN AC 47000; C: FGM with Zn addition in both alloys.

The lower microhardness in alloy EN AC 47000 after Zn addition in respect to the same alloy without Zn (bars #4 and #7, respectively) can be explained with the higher inhomogeneity detected in the alloy with Zn addition. In fact, such behaviour was not noticed in the FGMs interfaces with Zn, where microhardness resulted in improvement after Zn additions.

Considering the portion of EN AC 47000 in FGMs samples, the average microhardness measured was 78 ± 14, 74 ± 14 and 90 ± 20, respectively for FGM, FGM with Zn in EN AC 47000 and FGM with Zn in both compositions. These results seem to suggest that 1.5 w.t.% of Zn in EN AC 47000 does not significantly affect the alloy microhardness; on the other hand, Zn addition in both alloys causes an increase in microhardness of EN AC 47000 near the interface. This behaviour may be attributable to the higher Zn content detected near the interface between EN AC 51100 and EN AC 47000. The mixing of the compositions during the casting did not cause a depletion in Zn, because this constituent is present in both alloys.

Alloy EN AC 51100 has few alloying elements; thus, Zn addition may easily affect the average microhardness in this alloy, which increased from 60 ± 7 HV0.15 to 76 ± 3 HV0.15. Considering the portion of EN AC 51100 in FGM samples, the average microhardness measured were 71 ± 18, 67 ± 16 and 76 ± 11, respectively for simple FGM, FGM with Zn in EN AC 47000 and FGM with Zn in both compositions. These results suggest that Zn and the other alloying elements that characterize the alloy EN AC 47000 affect the microhardness of the alloy EN AC 51100. On the other hand, Zn addition only in alloy EN AC 47000 does not cause a further increase in EN AC 51100 microhardness, despite the composition mixing during the casting. Only the Zn addition in both alloys leads to an increase in microhardness.

The slight depletion of Mg and Zn at the interface of FGMs, detected in SEM-EDS maps in **Figures 4**, **6** and **8**, may explain the difference in microhardness measured respectively in the bulk alloy and near the FGM interfaces.

3.3.2 Tensile tests and fracture surfaces

Mechanical tensile tests were performed on FGMs specimens as well as on single alloy specimens.

Table 3 shows the tensile properties measured. FGMs are characterized by an average UTS (ultimate tensile strength) of almost 164 MPa, similar to FGMs with Zn addition. After adding Zn only in alloy EN AC 47000, the average UTS decreased to almost 151 MPa, while the elongation to fracture A% increased. In both cases, Zn addition caused a decrease of $R_{p0,2}$. In effect, in [20], the authors noticed that after adding 1.5–2% Zn, the mechanical UTS of Al-Si alloys decreases. Alloy EN AC 47000 affect the mechanical properties of all FGMs, regardless of the presence or absence of Zn. The alloy EN AC 47000 with Zn was characterized by almost 170 MPa of UTS, while the elastic module resulted very similar to the module of FGM with the addition of Zn only in EN AC 47000. Similarly, alloy EN AC 51100 with Zn has a UTS of about 148 MPa, as the UTS of FGM with the addition of Zn only in EN AC 47000. Zn addition in alloy EN AC 47000 seems not to affect UTS, resulting in slightly higher in the alloy without Zn; the same behaviour was previously noticed for the microhardness values.

EN AC 47000 has the higher average UTS, followed by EN AC 47000 with Zn and FGM without Zn. Not considering the average data, the higher UTS was detected for FGM specimen without Zn (184 MPa) while the lower was detected for alloy EN AC 51100 (122 MPa). As attended, alloy EN AC 51100 has shown the lowest mechanical properties and significant elongation to fracture A%.

In FGM specimens, it seems that $R_{p0,2}$ decreases with the addition of Zn. This behaviour goes against the solid solution hardening expected. In fact, Zn has a

$R_{p0,2}$ [MPa]	UTS [MPa]	A% [%]
FGM without Zn		
123 ± 20	164 ± 24	1.3 ± 0.6
FGM with Zn in EN AC 47000		
83 ± 0.6	151 ± 31	4 ± 3
FGM with Zn in both alloys		
99 ± 5	161 ± 20	2.8 ± 1
EN AC 47000 with Zn		
108 ± 3	171 ± 3	2 ± 0.02
EN AC 51100 with Zn		
111 ± 2	148 ± 27	2 ± 1
EN AC 51100		
73 ± 0.3	136 ± 21	6 ± 3.5
EN AC 47000		
108 ± 0.4	176 ± 9	2.5 ± 0.7

Table 3.
Average tensile tests results.

high solubility in the aluminium matrix. On the other hand, the $R_{p0,2}$ decreasing was only detected in FGMs specimens, while in alloy EN AC 47000 $R_{p0,2}$ remains almost constant and in alloy EN AC 51100 increases. In this sense, there are two possible explanations. First, the $R_{p0,2}$ decrease may be associated with a higher defect population in the FGM specimens that affect the yielding of the casting. The second hypothesis is that during the tensile test dislocations cannot pass through the Zn-straightened matrix and the primary Si particles, inducing concentrations of efforts that cause crack nucleation sites. The lower UTS after Zn addition may be similarly explained considering the additional presence of a certain defect population that affect the positive effect of Zn.

Particularly, the high standard deviation in the UTS of FGM without Zn addition was due to the presence of two specimens that fractured near casting defects. Such defects were primarily shrinkage porosities along the junction and in the proximity of the junction near the EN AC 51100. These porosities were caused by an incorrect elapsing time between the casting of the alloy EN AC 51100 and the subsequent pouring of EN AC 47000, causing air entrainment and mixing in the junction. Another important consideration must be done; notwithstanding FGM without Zn fractured preferentially in alloy EN AC 51100, the mechanical properties of the FGM without Zn still remain higher than the properties of the single alloy EN AC 51100 without Zn. This behaviour can be attributed to two reasons. The first one is that the presence of the alloy EN AC 47000, which is able to assure a high strength resistance, positively affects the FGM resistance, while the second is due to a good quality of the junction realized that provides a favourable stress distribution between the alloys.

Surface fractures were observed through SEM. In general, FGM specimens' rupture has occurred on the EN AC 51100 side; in one specimen, it occurs at the interface while, in one sample, the rupture was detected in alloy EN AC 47000 close to a defect. **Figure 11a** and **b** show fracture surfaces of two FGM without Zn. Mainly, **Figure 11a** shows the surface fracture of the FGM sample with the higher UTS, 188 Mpa. This specimen is characterized by a brittle fracture that occurred on alloy EN AC 47000. The fracture reveals a vast number of dendrites. **Figure 11b** displays an

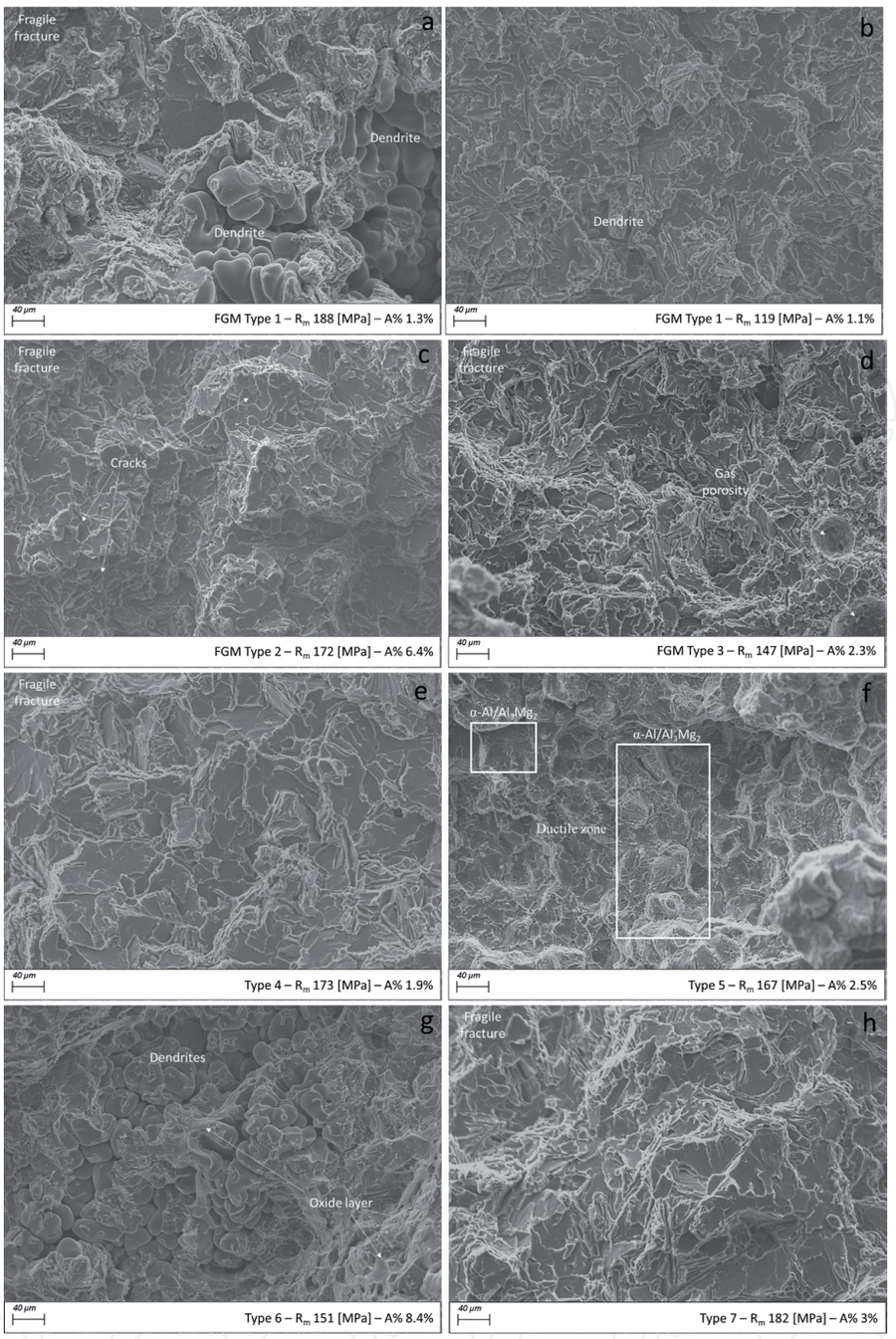


Figure 11.
Surface fractures for a few selected specimens. a, b: FGMs without Zn addition. c: FGM with Zn addition in EN AC 47000. d: FGM with Zn in both alloys. e,h: Alloys EN AC 47000 with and without Zn. f, g: Alloy EN AC 51100 with and without Zn addition.

FGM without Zn fractured along the interface between the alloys. A brittle fracture and dendrites characterize the fracture; this behaviour is symptomatic of a weak interface bonding between the two alloys. Overall, FGMs without Zn specimens are broken into the less resistant alloy, apart from specimens affected by casting issues.

Figure 11c and **d** show the fracture surfaces for both FGMs with Zn in EN AC 47000 and FGM with Zn in both compositions. Particularly, FGM with Zn only in EN AC 47000 fractured at the interface with pretty high elongation. On the other hand, FGM with Zn in both the alloys fractured with very low mechanical strength at the interface (147 MPa).

Figure 11e and **h** display the EN AC 47000, with and without Zn addition. Both fractures are brittle, and the elongation to fracture was approximately 2%. Cleavage plains were observed.

Alloy EN AC 51100 shows the highest elongation to fracture, of about 8%, while the elongation drops to about 2% after Zn addition. Despite the good mechanical properties, the elongation to fracture, in **Figure 11g**, is clearly visible extended dendrites. In **Figure 11f**, are visible the eutectic phases and a small amount of dimples.

Overall, intermetallic rod-like shapes or plate shapes cause brittle fractures for the concentration of efforts, as noticeable in **Figure 12**. Defects detected in surface fractures are mainly dendrites, but in FGM with Zn in both alloys were also noticed gas porosities. From the fracture analysis, it seems a certain grade of microporosity into the casting was realised, especially into alloy EN AC 51100. This behaviour was not previously highlighted in SEM analysis.

Near the rod-like intermetallics, are noticed cleavage plains. The very thin acicular microstructure of the eutectic regions α-Al/Al_3Mg_2 seems does not affect the rupture mode, resulting in an excellent elongation to fracture (**Figures 11f** and **12**).

3.3.3 Three-point bending test

Table 4 reports the results of bending tests for each specimen. As maximum values regard, FGM without Zn has the highest ultimate force F_{max} (394 Mpa). FGMs' deformation at rupture appears most influenced by alloy EN AC 47000 except for one sample, where the elongation resulted in about 10%.

FGM with Zn addition only in EN AC 47000 has shown the lower deformation at fracture and the lower Fmax; particularly, in sample #2, the $R_{p0,2}$ was so low that was not recorded. In FGM with Zn only in EN AC 47000, deformation at rupture is similar to deformation at rupture of alloy EN AC 51100, while in FGM with Zn in both alloys, it is similar to the deformation of alloy EN AC 47000.

Alloy EN AC 51100, as attended, has the highest deformation at rupture.

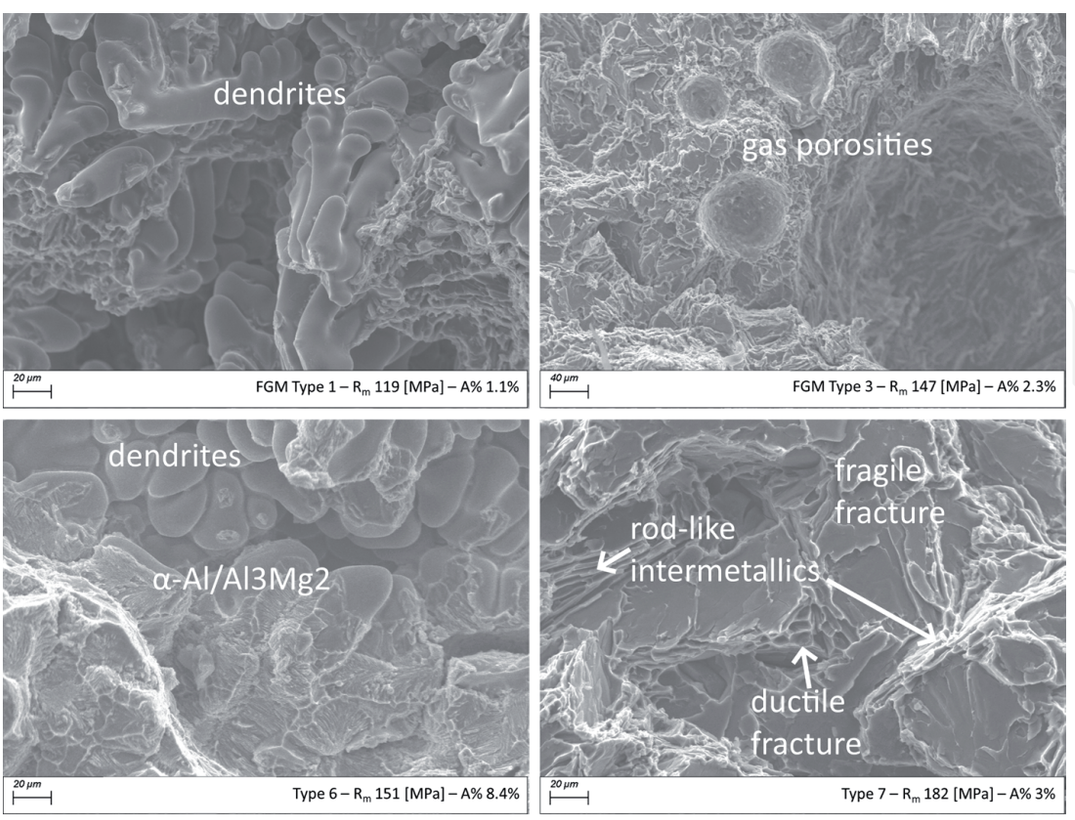


Figure 12.
Fracture details. FGM type 1 is the FGM without Zn; FGM type 3 indicates the FGM with Zn in both compositions; types 6 and 7 are alloys EN AC 51100 and EN AC 47000 without Zn.

Rp0,2 [MPa]	Fmax [MPa]	dL%
FGM without Zn		
181 ± 24	269 ± 65	5.6 ± 3
FGM with Zn in EN AC 47000		
191 ± 13	267 ± 45	4. ± 0.8
FGM with Zn in both alloys		
198*	151 ± 129 *	2.5 ± 0.2
EN AC 47000 with Zn		
183 ± 12	289 ± 24	2 ± 0.02
EN AC 51100 with Zn		
229 ± 16	306 ± 38	4 ± 0.9
EN AC 51100		
131 ± 8	318 ± 24	12.3 ± 0.9
EN AC 47000		
182 ± 11	347 ± 27	3.9 ± 0.7

Table 4.
*Three-point bending tests average results. * a brittle fracture affects both Rp0,2 (absence of yielding) and high standard deviation.*

As the three-point bending test regard, results are comparable with tensile tests. In fact, for example, FGMs in tensile conditions present similar UTS as the Fmax measured in FGM without Zn and with Zn in EN AC 47000. FGMs with Zn in both alloys resulted not comparable because of defects inside castings. Alloy EN AC 47000 has shown similar UTS with and without Zn, while in the bending test, the absence of Zn causes an increase in the specimen deformability, thanks to the lower solid solution straightening. Finally, EN AC 51100 bending behaviour is similar with or without Zn in terms of Fmax, despite the deformability decrease with Zn, as noticed for tensile test results.

3.3.4 Mechanical property connections

Average mechanical properties were compared to each other, and results are shown in graphs of **Figure 13**. **Figure 13a** shows a graph between the average ultimate tensile strength and the average elongation to fractures for each batch of samples. Graph a shows that alloy EN AC 47000 (type 4 with Zn and type 7 without Zn) has the highest R_m but low elongation to fracture. Conversely, alloy EN AC 51100 (type 5 with Zn and type 6 without Zn) have the lowest R_m, while A% changes as a function of Zn addition. Without Zn, EN AC 51100 castings reach the maximum average elongation.

As FGMs regard, Zn addition does not influence the R_m that remains almost constant, while dL% increases. The increase in dL% may be caused to the presence of nanoparticle intermetallic compounds Mg-Zn that positively affect the fracture mode, thanks to their rounded shapes [21]. Despite that, the intermetallic phases Mg-Zn are nanometric and, thus, are not easily observable at SEM. These intermetallic phases nucleate during the solidification; as the rate of Zn increases, the rate of Mg dissolved in α-Al decreases to form Mg-Zn intermetallic phases.

When comparing R_m to average microhardness values, as in **Figure 13c**, it becomes evident that EN AC 51100 castings have shown the higher R_m and higher microhardness, followed by FGM with Zn in both alloys and alloy EN AC 47000

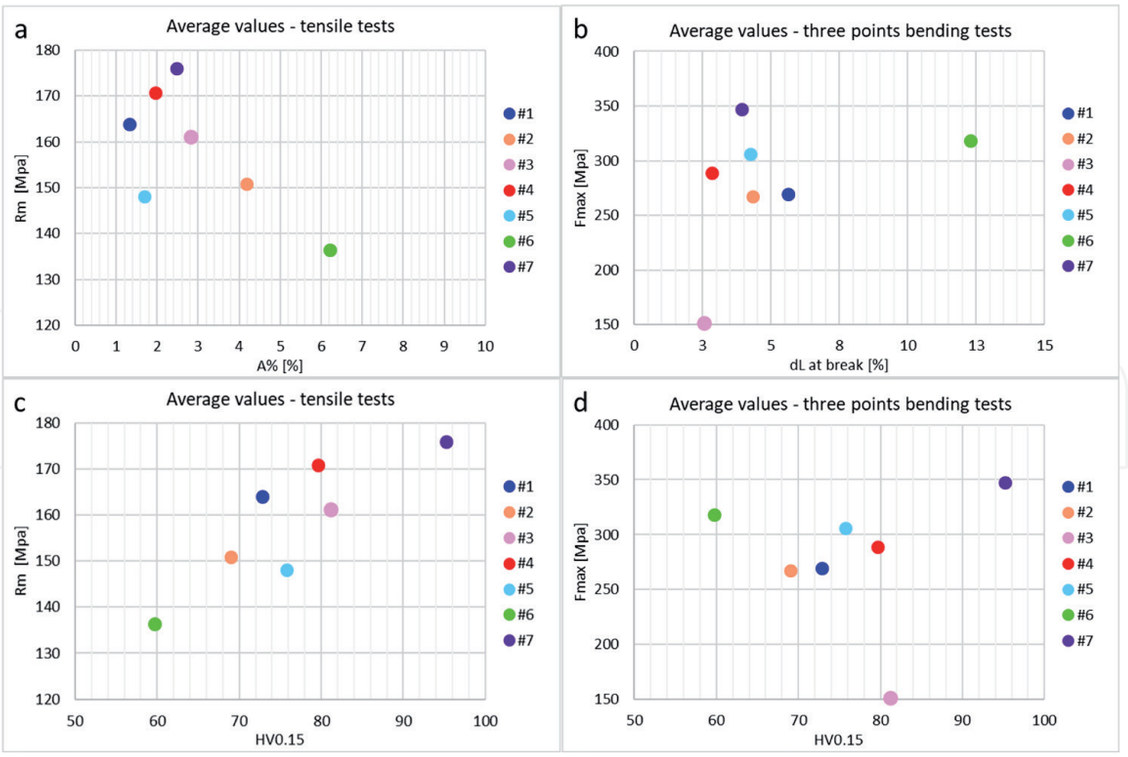


Figure 13.
Average values from **Tables 3** *and* **4**. *a: Average values Rm and A% obtained after tensile tests. b: Average values Fmax and dL% obtained after bending tests. c: Average values HV0.15 and Rm obtained after tensile tests and microhardness measurements. d: Average values HV0.15 and Fmax obtained after bending tests and microhardness measurements. FGM, FGM with Zn addition in EN AC 47000 and FGM with Zn addition in both alloys indicated as #1, #2, #3, while EN AC 47000 + Zn, EN AC 51100 + Zn, EN AC 47000, EN AC 51100 indicated as #4, #5, #6, #7.*

with Zn addition. On the other hand, as expected, EN AC 51100 castings present both the lowest R_m and microhardness. FGM with Zn only in EN AC 47000 presents a relatively low average R_m and microhardness; this was caused by a defective specimen that affects the batch's average values.

Figure 13b shows a graph between the maximum strength and the average deformation at ruptures dL% for each batch of samples. In both tensile and bending tests, EN AC 51100 has higher elongation/deformation at rupture (green points in **Figure 13a** and **b**), while EN AC 47000 specimens have the higher ultimate tensile strength/maximum force (violet points). FGM with Zn in both the alloys shows the lowest deformation at rupture. **Figure 13d** highlights the relation between the microhardness and the maximum force of bending tests; EN AC 47000 castings have the higher Fmax and higher microhardness, followed by alloy EN AC 47000 with Zn addition.

4. Conclusions

In this work, new kinds of functionally graded materials realized by controlling the mould filling were produced. The alloy Al-Si EN AC 47000 was adopted along with the Al-Mg composition EN AC 51100, obtaining castings with good-quality and low retained defects. The Zn addition was taken into account to increase the mechanical properties of the as-cast FGM, especially by nucleating the Mg-Zn intermetallic phases in composition EN AC 51100. Functionally graded materials were therefore produced in three variants—the first type was the simple casting of the two compositions; the second type involved the addition of commercially pure Zn into the Al-Si alloy, while the third type involved the Zn addition into both the

alloys composing the FGM. In order to better understand the FGM properties and compare the results, samples made in purely alloys Al-Si and Al-Mg were cast, with and without Zn addition, using the same production process of FGMs.

All the castings produced were mechanically tested, and their microstructures were observed at the scanning electron microscope SEM-EDS.

FGMs, realized by alloys Al-Si and Al-Mg, presented good bonding, which the mechanical testings have highlighted. Moreover, SEM observations of the FGMs interfaces highlight, in general, the absence of extended defects.

In alloy EN AC 51100 (**Figure 2**), intermetallic phases such as Al-Fe-Mn-Si phases, the eutectic α-Al/Al_3Mg_2 phase and Mg_2Si phase were found. In alloy EN AC 47000 (**Figure 3**), intermetallic Fe-Cu-Mn phase, Q phase, polygonal eutectic silicon and Chinese script α-AlFeSiCuMg were detected.

FGM interface is shown in **Figure 4**; intermetallic phases are coherent with those observed in **Figures 2** and **3**.

The silicon diffusion into Mg-based alloy was clearly noticeable, especially in the eutectic regions α-Al/Al_3Mg_2. Moreover, Mg was detected in both the alloys with a slight depletion at the interface, despite the single alloy EN AC 47000 was not containing Mg (see **Figure 7**). In the FGM with Zn addition in both alloys, either Zn adn Mg depletion at the interface were observed. The slight depletion of Mg and Zn at the interface of FGMs may explain the difference in microhardness measured respectively in the bulk alloy and near the FGM interfaces—in bulk alloys, microhardness appears higher with respect to microhardness near the interface.

Overall, the tensile strength and the maximum bending force seems to decrease with the addition of Zn. During the tensile test, probably, dislocations cannot pass through the Zn-straightened matrix, straightening intermetallic phases and primary Si particles, inducing concentrations of efforts that cause crack nucleation sites. The lower UTS after Zn addition may be explained considering the additional presence of a certain defect population that affect the mechanical properties.

IntechOpen

Author details

Elisa Fracchia[1*] and Mario Rosso[2]

1 Department of Applied Science and Technology, Polytechnic of Turin, Alessandria, Italy

2 INSTM c/o Department of Applied Science and Technology, Polytechnic of Turin, Alessandria, Italy

*Address all correspondence to: elisa.fracchia@polito.it

IntechOpen

© 2021 The Author(s). Licensee IntechOpen. This chapter is distributed under the terms of the Creative Commons Attribution License (http://creativecommons.org/licenses/by/3.0), which permits unrestricted use, distribution, and reproduction in any medium, provided the original work is properly cited. CC BY

References

[1] Li Y, Liu J, Zhang Q, Huang W. Casting defects and microstructure distribution characteristics of aluminum alloy cylinder head with complex structure. Materials Today Communications. 2021;**27**:102416. DOI: 10.1016/j.mtcomm.2021.102416

[2] Saleh B, Jiang J, Fathi R, Alhababi T, Xu Q, Wang L, et al. 30 Years of functionally graded materials: An overview of manufacturing methods, applications and future challenges. Composites Part B: Engineering. 2020;**201**:108376. DOI: 10.1016/j.compositesb.2020.108376

[3] Khan T, Zhang N, Akram A. State of the art review of functionally graded materials. In: Proceedings of the IEEE International Conference on Computing, Mathematics and Engineering Technologies (iCoMET 2019); 30-31 January 2019. Sukkur, Pakistan: IEEE; 2019. pp. 1-9. DOI: 10.1109/ICOMET.2019.8673489

[4] Sarathchandra DT, Kanmani Subbu S, Venkaiah N. Functionally graded materials and processing techniques: An art of review. Materials Today: Proceedings. 2018;**5**;10;1:21328-21334. DOI: 10.1016/j.matpr.2018.06.536

[5] El-Galy IM, Saleh BI, Ahmed MH. Functionally graded materials classifications and development trends from industrial point of view. SN Applied Sciences. 2019;**1**:1378. DOI: 10.1007/s42452-019-1413-4

[6] Ghanavati R, Naffakh-Moosavy H. Additive manufacturing of functionally graded metallic materials: A review of experimental and numerical studies. Journal of Materials Research and Technology. 2021;**13**:1628-1664. DOI: 10.1016/j.jmrt.2021.05.022

[7] Matuła I, Dercz G, Barczyk J. Titanium/Zirconium functionally graded materials with porosity gradients for potential biomedical applications. Materials Science and Technology. 2020;**36**(9):972-977. DOI: 10.1080/02670836.2019.1593603

[8] Vijaya Kumar P, Jebakani D, Velmurugan C, Senthilkumar V. Effect of SiC on mechanical and microstructural characteristics of Al based functionally graded material. SILICON. 2021. DOI: 10.1007/s12633-020-00933-0

[9] Marzuki M, Mazni Ismail N, Ihsan Abdul Latiff M. Preparation and microstructural characterization of five-layered aluminium-aluminium oxide functionally graded material. In: Proceedings of the 2nd International Conference on Innovative Technology, Engineering and Sciences (iCITES 2020); 22-23 December 2020. Vol. 1092. Pekan Pahang, Malaysia: IOP Conference Series: Materials Science and Engineering; 2021. p. 012031. DOI: 10.1088/1757-899X/1092/1/012031

[10] Surya MS, Prasanthi G. Effect of silicon carbide weight percentage and number of layers on microstructural and mechanical properties of Al7075/SiC functionally graded material. SILICON. 2021. DOI: 10.1007/s12633-020-00865-9

[11] Mallick A, Gangi Setti S, Sahu RK. Centrifugally cast A356/SiC functionally graded composite: Fabrication and mechanical property assessment. Materials Today: Proceedings. 2021;**47**:11. DOI: 10.1016/j.matpr.2021.07.155

[12] Elkotb HH, Mostafa R, Samad AAA, Enab TA. Manufacturing and characterization of functionally graded material automotive piston using centrifugal casting technique. Solid State Phenomena. 2021;**3**(318):13-24. DOI: 10.4028/www.scientific.net/SSP.318.13

[13] Pradeep AD, Rameshkumar T. Review on centrifugal casting of functionally graded materials. Materials Today: Proceedings. 2021;**45**:729-734. DOI: 10.1016/j.matpr.2020.02.764

[14] Karun AS, Sanil H, Rajan TPD, Pillai UTS, Pai BC. Characteristics of functionally graded bimetallic aluminium alloys by sequential casting technique. Materials Science Forum. 2015;**830-831**:383-386. DOI: 10.4028/www.scientific.net/MSF.830-831.383

[15] Kieback B, Neubrand A, Riedel H. Processing techniques for functionally graded materials. Materials Science and Engineering A. 2003;**362**(1-2):81-105. DOI: 10.1016/S0921-5093(03)00578-1

[16] Król M, Tański T, Snopiński P, Tomiczek B. Structure and properties of aluminium–magnesium casting alloys after heat treatment. Journal of Thermal Analysis and Calorimetry. 2017;**127**:299-308. DOI: 10.1007/s10973-016-5845-4

[17] Fracchia E, Lombardo S, Rosso M. Case study of a functionally graded aluminum part. Applied Sciences. 2018;**8**:7. DOI: 10.3390/app8071113

[18] Fracchia E, Gobber FS, Rosso M, Actis Grande M, Bidulská J, Bidulský R. Junction characterization in a functionally graded aluminum part. Materials (Basel). 2019;12;21:3475. DOI: 10.3390/ma12213475

[19] Ebhota WS, Jen T-C. Intermetallics formation and their effect on mechanical properties of Al-Si-X alloys. In: Aliofkhazraei M, editor. Handbook of Intermetallic Compounds - Formation and Applications. Rijeka: IntechOpen; 2017. DOI: 10.5772/intechopen.73188

[20] Němec M, Gärtnerová V, Klementová M, Jäger A. Analysis of intermetallic particles in Mg-12 wt.%Zn binary alloy using transmission electron microscopy. Materials Characterization. 2015;**106**:428-436. DOI: 10.1016/j.matchar.2015.05.038

[21] Alemdag Y, Beder M. Effects of zinc content on strength and wear performance of Al–12Si–3Cu based alloy. Transactions of the Nonferrous Metals Society of China. 2019;**29**(12):2463-2471. DOI: 10.1016/S1003-6326(19)65154-X